Synthetic modification of fusogenic coiled coil peptides

Crone, N.S.A.

3.

Modulation of coiled-coil binding strength and fusogenicity through peptide stapling.

This chapter was published as an original research paper: Niek S.A. Crone, Alexander Kros, Aimee L. Boyle, Bioconjugate Chemistry **2020**, 31, 3, 834–843.

Abstract

Peptide stapling is a technique which has been widely employed to constrain the conformation of peptides. One of the effects of such a constraint can be to modulate the interaction of the peptide with a binding partner. Here, a cysteine bis-alkylation stapling technique was applied to generate structurally isomeric peptide variants of a heterodimeric coiled-coil forming peptide. These stapled variants differed in the position and size of the formed macrocycle. C-terminal stapling showed the most significant changes in peptide structure and stability, with calorimetric binding analysis showing a significant reduction of binding entropy for stapled variants. This entropy reduction was dependent on crosslinker size and was accompanied by a change in binding enthalpy, illustrating the effects of preorganization. The stapled peptide, along with its binding partner, were subsequently employed as fusogens in a liposome model system. An increase in both lipid-, and content-mixing was observed for one of the stapled peptide variants: this increased fusogenicity was attributed to increased coiled-coil binding but not to membrane affinity; an interaction theorized to be a primary driving force in this fusion system.

3.1 Introduction

Intramolecular crosslinking of peptides, commonly referred to as peptide stapling, is often employed to change or constrain the secondary structure of small peptides and to induce unstructured peptides to mimic complex protein folds and protein-protein interactions(PPIs).[1-4] Stapling also contributes to an increased resistance to denaturation and proteolytic degradation, making it a useful technique for the modification of peptide-based therapeutics.[5] Hydrocarbon stapling, a technique which is based on catalyzed olefin metathesis, has seen widespread application with multiple compounds being investigated in academic, pre-clinical and clinical studies.[6-10]

Peptide stapling techniques can be broadly divided into two categories: single- and two-component strategies. Single-component strategies incorporate amino acids that can be cross-linked selectively, or protection strategies are chosen that allow selective crosslinking. Common single-component stapling strategies include disulfide bonding,[11] lactam bridges,[12, 13] and olefin metathesis.[10] Two-component stapling adds a bifunctional crosslinker to bridge two amino-acid side chains; the most common techniques are based on cysteine crosslinking and triazole linkages.[14-17] Two-component strategies are in principle more complex than single-component strategies, but allow for a more flexible crosslinker design as it does not need to be compatible with solid-phase peptide synthesis. Although most stapling techniques are used to increase or constrain peptide helicity, systems that compare different methods are often based around short peptide sequences, and although multiple comparisons have been made,[18, 19] the ideal crosslinking technique is still open to debate.[20]

The α-helix secondary structure motif has been mimicked using stapled peptides due to its common occurrence in proteins, and therefore its potential as a PPI mimic.[21] Coiled coils, which are protein-folding motifs comprising two or more α-helices, are intrinsically helical and therefore techniques commonly used for the stapling of helices should permit modulation of coiled-coil interactions. Indeed, Rao *et al.* has shown lactam bridges can be used to generate short, helical, cFos binding peptides,[22] and Haney and Horne have used oxime crosslinking to generate stapled variants of the GCN4-p1 coiled-coil domain.[23] More recently, Wu *et al.* used a bis-triazole stapling technique to increase peptide binding to the polymerase α

accessory factor ctf4,[15] and Lathbridge and Mason showed that lactam-bridged heptapeptides can be used for the *de novo* design of a coiled-coil binding peptide.[24]

Together, these studies provide methods for the crosslinking of coiled-coil or coiled-coil-binding peptides, but it is unclear which method would prove most effective when applied to a different coiled-coil system. The size of the macrocycle formed varies significantly between the different cross-linking techniques, as do the polar and hydrophobic interactions of the crosslinkers in question. Interactions of the asymmetric oxime moiety with different amino acid side chains resulted in different binding strengths when the crosslinker was reversed in Haney and Horne's method. This necessitated the preparation and evaluation of both variants, and indicates oxime crosslinking effectiveness is dependent on amino acid composition.

The choice of crosslinking technique was therefore not obvious when attempting to modulate the behavior of the heterodimeric coiled coil used in our group, consisting of two peptides with a triple heptad repeat sequence of opposing charge, used as components of a membrane fusion model system.[25] The position of the crosslinker and the macrocycle size were deemed the most influential characteristics in the previously mentioned crosslinking strategies, therefore we wanted to evaluate both of these criteria independently for our system. The most favorable candidates could then be used to test the effect of structural changes on coiled-coil-based membrane fusion. One stapling strategy that attracted our attention was developed by the DeGrado lab, and is based on the alkylation of cysteine using dibromoxylenes.[26] The advantage of this system lies in the rigidity provided by the aromatic ring, allowing precise spacing between the two thiol moieties by selecting one of the three different structural isomers of dibromoxylene: *ortho; meta;* and *para*, **Scheme 3.1**. In the original study *meta*-xylene showed the most promise as a crosslinker, and further investigations in the same group have therefore focused on this variant.[27, 28] Other recent investigations have also predominantly used the *meta* derivative,[29, 30] and when a comparison was made between the isomers, only short or unstructured peptides were used. This means the question of whether, for a helical or coiled-coil peptide, *meta*-xylene is indeed the best crosslinking moiety is unanswered. Therefore, to probe the effect of stapling on coiled-coil peptides, we elected to investigate dibromoxylene crosslinking of cysteine's, employing all three structural isomers in order to elucidate the role of crosslinker size and its effect on structure and activity.

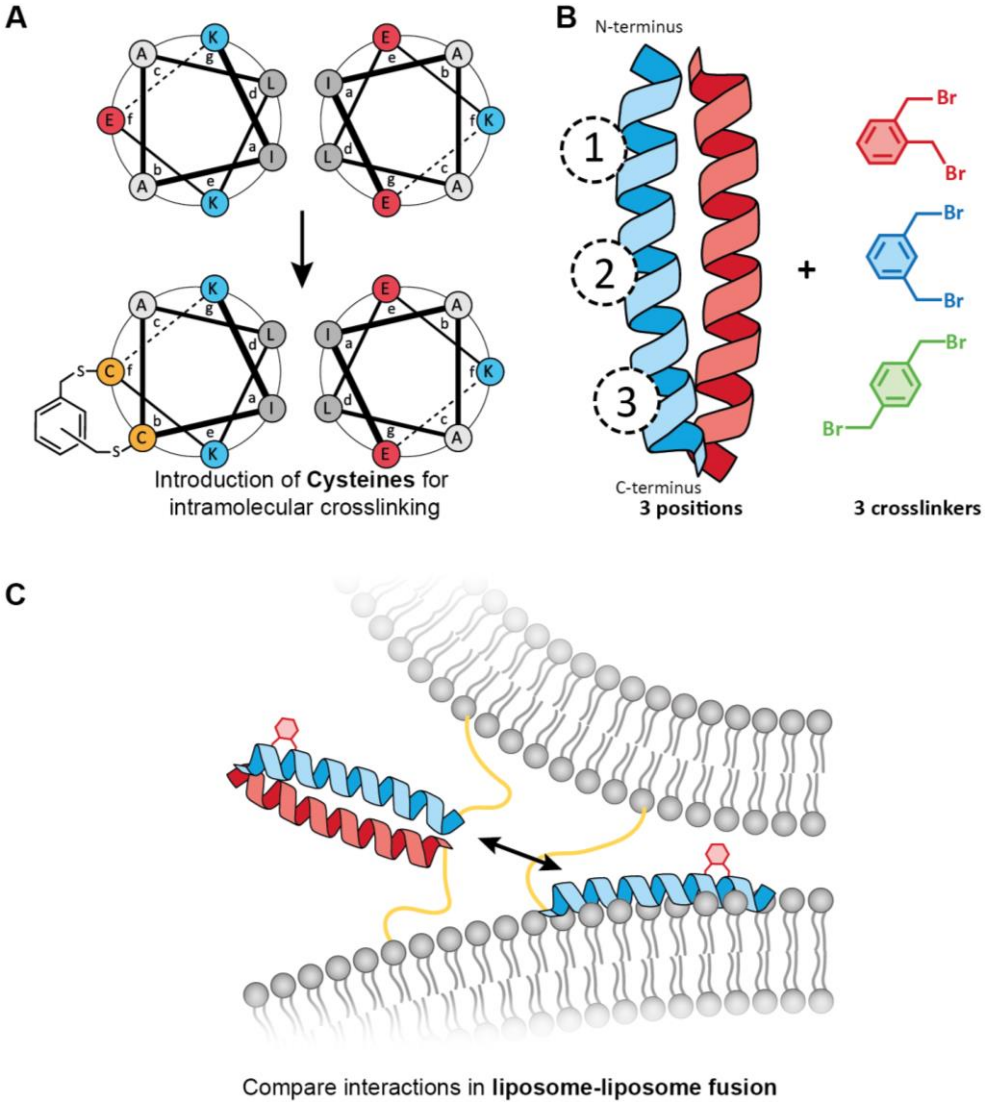

Scheme 3.1. The peptide stapling strategy used in this paper. (A) Two solvent-exposed amino acids are replaced with cysteine and crosslinked using a xylene moiety. (B) The relative positioning of three different crosslinking sites and the structures of the dibromoxylene crosslinkers investigated in this project. (C) A schematic representation of the studied membrane fusion interactions; coiled-coil formation and membrane insertion.

The fusion system developed in our lab is inspired by naturally occurring SNARE (soluble NSF attachment protein receptors) proteins,[31] and consists of a pair of complementary peptides. These peptides are dubbed E and K, and form a heterodimeric coiled-coil that has be attached to lipid membranes via a PEG spacer and lipid anchor.[32] Like SNARE proteins this model system promotes the fusion of

lipid membranes, and it can be facilely modified to study the process of membrane fusion via structure-activity relationships.[33] It has recently been discovered that these two peptides play different roles in the fusion process.[34] The interactions of the K peptide with lipid membranes have been hypothesized as an important factor in membrane fusion efficiency.[35] Membrane interactions can occur simultaneously with formation of the coiled-coil domain in a membrane fusion interface (as visualized in **Scheme 3.1C**), therefore a fine balance between the two must be achieved. In addition, both membrane binding and coiled-coil formation depend on the peptides adopting a helical structure; we believe stapling should allow for the generation of peptides with varied helical structures, which will in turn affect coiled-coil formation and membrane binding interactions. Studying the effects of modulating the membrane interactions and coiled-coil binding affinity will generate insights into the importance of both factors in membrane fusion.

In this study, a library of nine stapled peptides was prepared by modifying peptide K via cysteine alkylation. These stapled K-peptide derivatives exhibited systematic variations in helicity and thermal stability, as observed by circular dichroism (CD) spectroscopy. The coiled-coil binding thermodynamics were studied using isothermal titration calorimetry (ITC) and it was discovered that increased coiled-coil binding is based on a preorganization effect. These observed changes in structure and binding dynamics were heavily dependent on the location of the staple and the choice of crosslinker. In lipid-, and content-mixing experiments a significant change in fusogenicity was measured for selected stapled peptides, which was attributed to the altered coiled-coil interaction strength.

3.2 Results and Discussion

Stapled Peptide Design

The starting point for structural modification is one peptide of a three-heptad heterodimeric coiled-coil pair first reported by Litowski and Hodges.[36] The two peptides are named after the abundance of either glutamic acid (Glu, E) or lysine (Lys, K) respectively, and each peptide contains a C-terminal glycine and either tyrosine or tryptophan as a fluorescent reporter, giving rise to E_3GY and K_3GW. To facilitate stapling two amino acids in peptide K_3GW were modified to cysteine, spaced *i* to *i+4* to best match a single α-helical turn. Amino acids that are involved in electrostatic (positions *e* and *g*) or hydrophobic (positions *a* or *d*) interactions

were not varied to ensure the stapled peptides retained the same stabilizing coiled-coil interactions as the parent peptides.

Three different variants were generated each with the cysteines, and therefore the staple, in a different heptad, shown in **Table 3.1**. Each of these positional variants was stapled with *ortho*-, *meta*-, and *para*-dibromoxylene generating a library of nine stapled peptides. When referring to these stapled peptide variants, a notation which reflects the position and type of crosslinker is used, for example K_3GW-1*M* signifies the crosslinker is in the first heptad and the *meta* variant has been employed.

Table 1. Sequences of the coiled-coil parent peptides and cysteine-containing variants.

Peptide	**Sequence**				
	g	*abcdefg*	*abcdefg*	*abcdefg*	*a*
E_3GY	E	IAALEKE	IAALEKE	IAALEKG	Y
K_3GW	K	IAALKEK	IAALKEK	IAALKEG	W
K_3GW-1	K	I**C**ALK**C**K	IAALKEK	IAALKEG	W
K_3GW-2	K	IAALKEK	I**C**ALK**C**K	IAALKEG	W
K3GW-3	K	IAALKEK	IAALKEK	I**C**ALK**C**G	W

Secondary structure analysis

CD spectroscopy was employed to determine the secondary structure of the stapled peptide variants; the effects of both stapling location and the size of the crosslinker can be clearly observed, **Figure 3.1** & **Figure S3.1**. Peptide stapling close to the C-terminus (K_3GW-3 variants) showed the largest increase in α-helicity for all three xylenes, whereas modification in the second heptad (K_3GW-2 variants) showed the lowest increase. Notably, when *para*-xylene was used as the crosslinker in the second heptad, the overall peptide helicity was reduced, **Figure 3.1B**, showing para-xylene is too large to form an ideal α-helix. The N-terminal positions (K_3GW-1 variants) all show a moderate increase in helicity, largely independent of staple size, confirming the previously observed trend for hydrocarbon stapling to be most effective at peptide termini.[37] Using temperature-dependent CD spectroscopy, an increase in melting temperature (T_m) could be determined for the stapled peptide variants, as shown in **Figure 3.2** and **Figure S3.2**,

with the change in T_m closely following the observed changes in helicity. C-terminal modification showed the largest increase in melting temperature, with the *ortho*-xylene crosslinker yielding the most stable peptides over all three peptide variants, followed by the *meta*-xylene crosslinker. All stapled peptides interacted with E_3GY, showing typical coiled-coil spectra as is evident in **Figure 3.1C** and **Figure S3.1**. C-terminal stapling showed the highest helicity, while the N-terminal stapled peptides did not have increased coiled-coil helicity compared to the staples located in the central heptad.

In contrast to the stapled peptides in isolation, *meta*-xylene-modified peptides show the most α-helical structure as a coiled coil. O*rtho*-xylene stapled peptides

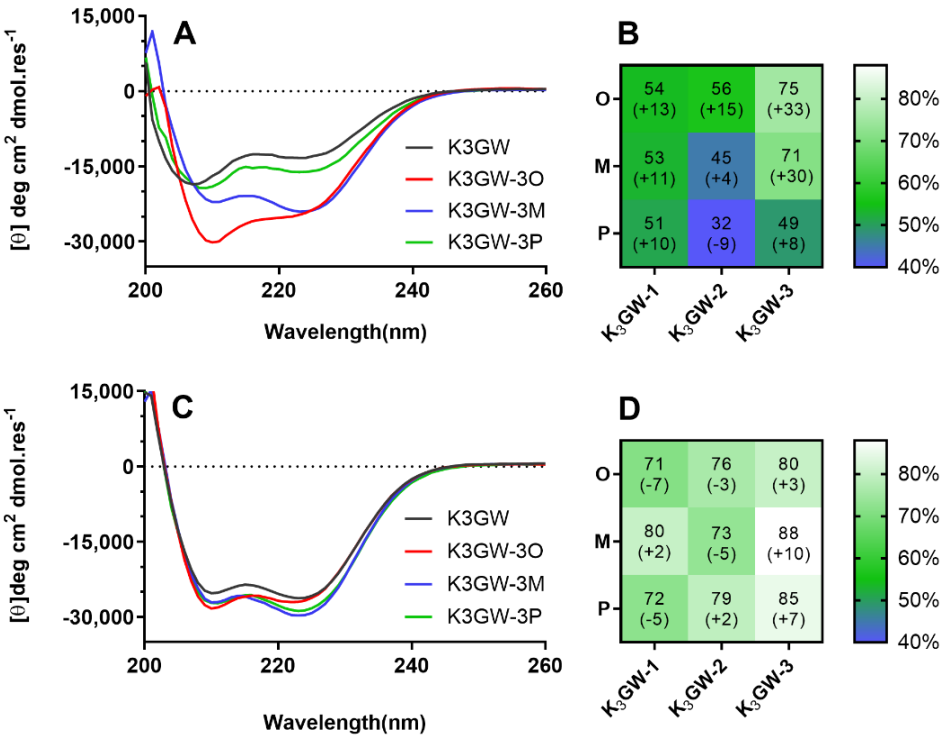

Figure 3.1. CD spectra of stapled peptides. (A) CD spectra of C-terminal stapled peptides, (B) heat map of the percentage of peptide helicity for all stapled variants and the change in helicity compared to K_3GW in brackets, (C) CD spectra of the C-terminal stapled peptides mixed with peptide E_3GY to form a coiled coil, and (D) heat map of average peptide helicity of all stapled peptides when combined with peptide E_3GY and the change in helicity compared to the coiled-coil with K_3GW in brackets. Total peptide concentration is 50 µM, spectra were recorded at 20˚C in pH 7.4 PBS buffer.

had the largest increase in T_m for all three positions (**Figure 3.2**), and the trends in coiled-coil stability are similar to those observed for the single peptides, with an average increase in T_m of 4.9˚C for the stapled peptides, (**Table S3.1**) and 4.8˚C for their coiled coils, (**Table S3.2**). *Meta*-xylene was previously shown to have the largest increase in helicity in small unstructured peptides,[26] but in the E/K system *ortho*-xylene stapled variants yielded the highest single-peptide helicity and largest increase in T_m for both the peptides and their respective coiled-coils. Because it is possible that stapling affects coiled-coil interactions without changing peptide helicity as observed via the thermal unfolding experiments, the effect of peptide stapling on coiled-coil binding was further investigated using isothermal titration calorimetry (ITC).

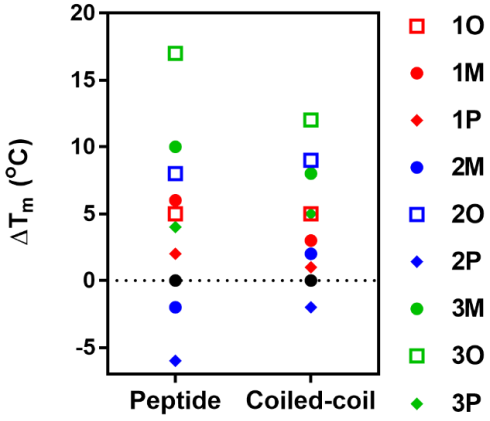

Figure 3.2. Change in peptide (left) and coiled-coil (right) melting temperature for stapled peptides in comparison to K_3GW as determined via CD spectroscopy. Total peptide concentration is 50 µM C in pH 7.4 PBS buffer, spectra were recorded from 5 to 95˚C and are shown in **Figure S3.2**.

Binding thermodynamics of stapled coiled-coils

Direct determination of the dissociation constant (K_d) and enthalpy of binding (ΔH_b), and therefore calculation of the free energy (ΔG_b) and entropy of binding (ΔS_b) is possible using ITC (**Figure S3.3**), allowing investigation of peptide interactions independent of peptide structure.[38] The results shown in **Figure 3.3** and **Table S3.3** show that, in general, coiled-coil binding of peptides K_3GW and E_3GY is strongly enthalpically favored but entropically unfavored. The effect of enthalpy can be explained via the formation of amide hydrogen bonds and electrostatic interactions upon folding of the peptide.

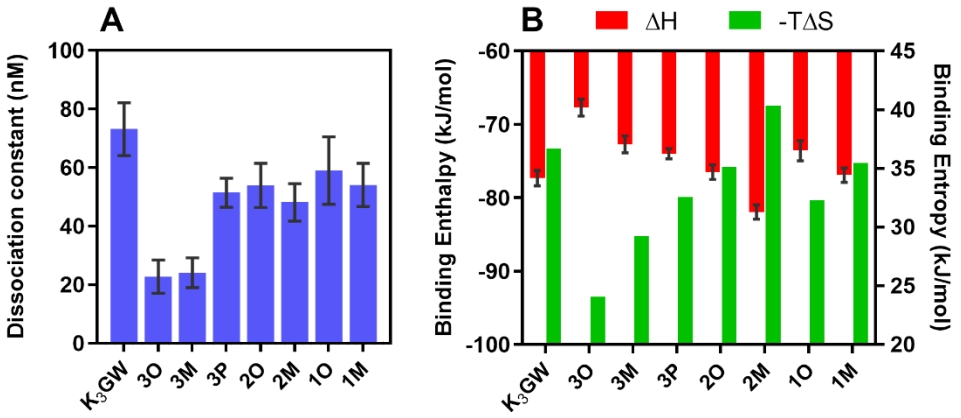

Figure 3.3. Thermodynamic binding parameters of K_3GW and its stapled derivatives in complex with E_3GY, determined via ITC. Error bars show the fitting error to a single-binding site model for both (A) the dissociation constant, and (B) the binding enthalpy (ΔH). The entropy (-TΔS) is calculated from these parameters, and no error bars are drawn.

When the C-terminally-stapled variants of peptide K_3GW are analyzed, the K_d is decreased from 73 nM to 22 and 24 nM for the 3*O* and 3*M* variants respectively, and to 51 nM for the 3*P* variant. A large decrease in ΔS_b was observed and was directly related to the size of the implemented staple. *Ortho*-xylene stapling at the C-terminus reduced the effect of entropy upon binding from 37 to 24 kJ/mol, a reduction of 35%. At the same time, an increase in the ΔH_b from -77 to -68 kJ/mol was observed, counteracting the observed entropic effects and leading to the conclusion that the mechanism of peptide stapling relies on a preorganization effect. Through conformational restriction, the peptide is preorganized in a helical conformation which reducing the entropic effects on binding, but the potential energy that is gained upon formation of an α-helix is also lost. Although the K_d for the C-terminal *ortho-,* and *meta*-xylene stapled peptides are comparable, the ΔS_b is more favorable for the *ortho* variant, explaining the large differences in T_m observed for these two peptides. At all three stapling positions, the *ortho* variants show a reduced effect of entropy upon binding compared to the *meta* variants, which is likely caused by the smaller size of the *ortho* crosslinker. A smaller crosslinker restricts the maximum distance between the two helical turns, and therefore limits the number of possible conformations that the peptide can assume.

Recently, Miles *et al*. screened hydrocarbon-stapled peptides as protein-protein interaction (PPI) mimics against Bcl-x_L/Mcl-1 and observed similar changes in the

ΔH_b and ΔS_b for their stapled peptides, however they observed an overall increase in ΔG_b.[39] Binding kinetics determined via a surface plasmon resonance (SPR) assay showed that the binding of their PPI mimic could best be explained via an induced fit mechanism, where the PPI can interact via multiple binding modes. Restricting the potential conformations of the peptide through the introduction of a staple reduced the number of possible binding modes, and therefore increased the overall K_d of the system. The E/K peptides used in this paper are designed, and experimentally confirmed to form heterodimeric coiled-coils exclusively.[40] As there is only one binding mode the observed changes in structure and stability, as determined via CD, show a direct correlation with the binding thermodynamics in ITC: C-terminal stapling using *ortho* and *meta*-xylene is the most effective way to increase the binding strength of coiled-coil peptides.

Membrane interactions of peptide K3GW are perturbed by peptide stapling

The effectiveness of E/K-based membrane fusion is partially attributed to the membrane interactions of peptide K, which are theorized to induce membrane curvature and therefore accelerate the transition from membrane docking to hemifusion.[41] The interactions of peptide K with lipid membranes are based on a lysine snorkeling mechanism, which describes the hydrophobic amino acids in the '*a*' and '*d*' positions inserting in a lipid membrane, helped by the favorable electrostatic interactions between lysine's and the phosphate groups of the lipid membrane.[42] This is a reversible process that can only happen when the peptide folds into an amphipathic helix and all the hydrophobic amino acids are positioned on the same face. Peptide stapling, which changes the overall peptide conformation, is therefore theorized to have an effect on membrane binding. The membrane partition coefficient (K_p) of the stapled K variants was assayed via tryptophan fluorescence titration experiments, and the results are shown in **Figure 3.4.** Membrane binding is either comparable to unmodified K_3GW or was increased up to a factor of two, and did not show any correlation to the location of the staple or to the overall helicity of the peptide (**Figure S3.4**). The difference in partition coefficient between K_3GW-3*O* and K_3GW-3*M* is striking, as the value is almost half for the *ortho* variant despite the helicity of the two being very similar. This shows that the addition of a hydrophobic crosslinking moiety between the *'b'* and *'f'* positions does not increase the membrane affinity of amphiphilic α-helical peptides in a structure-dependent manner, and leads to the hypothesis that peptide K_3GW does not bind to liposomal membranes as a highly structured α-helix.

CD experiments were performed with the C-terminal stapled peptides in the presence of liposomes, and this data showed a reduced ellipticity at 222 nm, and a high 208/222 nm ratio (see **Figure S3.6**). This indicates that the peptides are less α-helical in the presence of liposomes, which supports this hypothesis. If partitioning from the aqueous phase into the membrane is assumed to require partial unfolding of the peptide helix, the difference in binding strength between the *ortho* and *meta* variants can also be explained by the smaller size of the *ortho* crosslinker, which restricts the ability of the peptide to unfold.

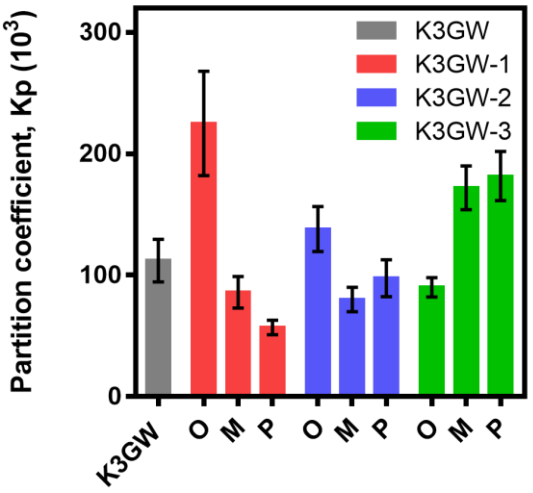

Figure 3.4. Partition coefficient of peptides with liposome membranes. Partition was measured via tryptophan fluorescence titration at 20 ˚C in pH 7.4 PBS buffer. Error bars represent the error in fitting of K_p. Values and fitting of the titration data can be found in **Table S3.4** and **Figure S3.5**.

Lipid- and content-mixing is increased for C-terminal stapled peptides

Complete fusion of two lipid-membrane-enclosed spaces will result in homogenous mixing of the lipids in the inner and outer leaflets, as well as mixing of the inner contents. In a liposomal system this process can be studied via the incorporation of chromophores into the lipid bilayer or on the inside of the liposomes.

Fusion of these liposomes with non-labeled liposomes will result in a fluorescence change which can be quantified to compare the peptide fusogenicity. Lipopeptides were prepared which contained cholesterol and a polyethyleneglycol (PEG_4) spacer at the N-terminus, facilitating membrane anchoring.[43] Stapled peptides K_3GW-*3O*

and K_3GW-*3M* were selected for fusion studies because these gave rise to the largest structural and thermodynamic changes. Moreover, their binding strength is comparable but their partition coefficient differs by a factor of two therefore by testing both, and comparing them to unmodified K_3GW, the effect of both coiled-coil binding strength and membrane binding on fusogenicity can be determined. The lipopeptides were prepared using a novel on-resin stapling technique enabled by the use of 4-Methoxytrityl (Mtt) protected cysteine, full details are available in the materials and methods section. These peptides were tested for fusogenicity together with the lipidated variant of E_3GY (structures can be found in **Scheme S3.1**).

Lipid mixing was quantified using a Förster resonance energy transfer (FRET) pair incorporated in the lipid membrane, the results are shown in **Figure 3.5A**. The amount of lipid mixing observed was comparable for K_3GW and K_3GW-3*M* at a 1% peptide concentration, while the K_3GW-3*O* variant showing increased lipid mixing six minutes after the start of the experiment. This indicates that docking of the liposomes occurs at the same speed, but more lipid mixing occurs for the K_3GW-3*O*

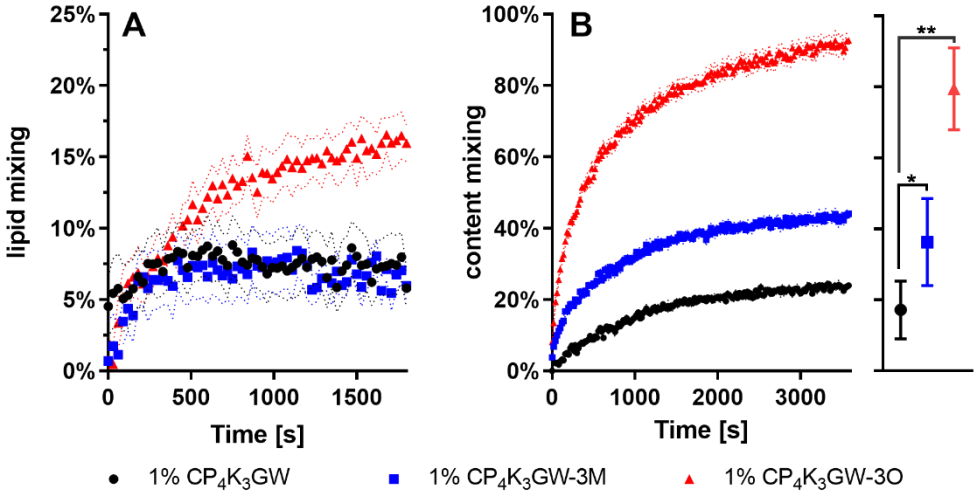

Figure 3.5. (A) Lipid mixing and (B) content mixing experiments of liposomes decorated with stapled peptides. Graphs show the change in mixing over time, and the standard deviation between 4 samples followed simultaneously. The dot bar graph (right) represents the average content mixing and deviation over 3 separate experiments. Experiments were performed at 500 μM total lipid concentration in pH 7.4 PBS at 20 ˚C. Fusion experiments were performed at 1% lipopeptide concentration and fluorescence was normalized against 0% and 100% control samples.

variant. As the absolute amount of lipid mixing was low, the same experiment was also performed with 2% of the lipopeptides, which doubled the amount of lipid mixing observed while retaining the same trends (**Figure S3.7**).

Content mixing experiments when performed properly are the best measure for complete fusion of two lipid membranes. The membrane-impermeable sulforhodamine B (SrB) dye was employed as a fluorescent reporter and showed significant increases in fusion for both stapled peptide variants, **Figure 3.5B**, with the K_3GW-3*M* variant doubling the amount of content mixing compared to K_3GW (from 17.1% to 36.2%). The K_3GW-3*O* variant produced an even larger increase; up to 93% content mixing was observed after 60 minutes, with an average of 79.5%. This is surprising, since there was no observed difference between K_3GW and the K_3GW-3*M* variant during lipid mixing experiments. An immediate difference between the three peptides is observed at the start of the experiment, which is not the case for lipid mixing, raising the concern that the stapled peptide variants might be destabilizing the liposomes and cause leakage of SrB across the lipid membranes. Plain liposomes and liposomes modified with 1% lipidated E_3GY were tested for leakage but did not show significant differences (**Figure S3.8**), indicating that the stapled peptides do not destabilize the liposomal membranes.

Insights into the mechanism of coiled-coil based membrane fusion

Membrane fusion occurs in multiple stages, starting with the docking of two membranes to create a membrane fusion interface, followed by hemifusion which results in the mixing of the outer lipid leaflets, and proceeding via the formation of a fusion pore to complete fusion of the two liposomes, meaning their contents are exchanged.[33] Both lipid- and content-mixing experiments showed increased fusogenicity for the lipidated K_3GW-3*O* peptide, with increased content mixing also observed for the K_3GW-3*M* variant. Differences in lipid-mixing amount are obvious after six minutes, indicating that the rates of initial docking and outer leaflet mixing is comparable for the three peptides. Because complete fusion of the liposomes, as judged by content mixing, is increased significantly for the K_3GW-3*O* variant, the observed difference in lipid mixing is most likely caused by an increased mixing of the inner leaflet lipids. The increased coiled-coil binding strength observed via ITC, could explain the increase in fusion except for the fact that K_3GW-3*O* and K_3GW-3*M* are dissimilar in their fusogenicity, yet they have a comparable K_d. The K_3GW-3*O* and K_3GW-3*M* stapled peptides differ in their effects of entropy on coiled-coil binding and the strength of their membrane interactions, which are both increased

for K_3GW-3*M*. The K_d of coiled-coil formation is dependent on the association and dissociation rate constants, which show different behavior in temperature dependent stopped-flow experiments of coiled-coil peptides.[44] The dissociation rate was shown to be more dependent on temperature, and therefore had a much larger entropic component then the rate of association. The stapled peptide variants tested have a decreased entropic binding component, and should therefore also show a lower rate of dissociation. In a membrane fusion interface, dissociation of the coiled-coil is most likely followed by either another peptide binding event, or by the insertion of peptide K into the lipid membrane. A decrease in the dissociation rate should therefore result in an increase in the rate of fusion, although the total amount of fusion observed is not expected to change.

For SNARE-mediated membrane fusion it is known that multiple protein complexes are required to drive fusion of a single vesicle, and the likelihood of fusion occurring is dependent on the number of protein complexes at the fusion interface.[45, 46] This cooperativity is likely also necessary for our coiled-coil based system, and any interactions that influence the amount of coiled-coils that can be co-assembled around a fusion interface will influence the amount of fusion observed. In this case, both K_3GW-3*O* and K_3GW-3*M* show increased binding and lowered binding entropy, and therefore increased fusion via a lower dissociation rate. For K_3GW-3*M* this difference is less significant, and is likely to be partially counteracted by the increased membrane affinity of the peptide. This is a competitive interaction in the formation of the coiled-coil complex, and an interaction which can provide a pathway for dissipation of the free peptide after dissociation of the coiled coil.[41] In this manner, the total number of peptide complexes that are formed around a membrane fusion interface is reduced, and no increase in membrane fusion is observed. This reasoning can also be applied to homomeric peptide interactions, which could provide a pathway for dissipation of the lipopeptide away from the fusion interface. A CD titration was performed with K_3GW and the K_3GW-3*O* and K_3GW-3*M* analogues to test for homodimerization (**Figure S3.9** and **Table S3.5**), but the dimerization constant was found to be comparable for all variants, and weak enough that this should not be considered an important part of the fusion mechanism. This mechanistic understanding derived from the observed differences between the two stapled peptide variants will require further confirmation in different systems and experiments.

3.3 Conclusions

We have employed a cysteine bisalkylation stapling technique to generate of a series of nine structurally isomeric α-helical peptides that can form a heterodimeric coiled-coil when mixed with their binding partner. CD and ITC experiments showed that both stapling location and choice of staple affected the properties of the resulting peptides and coiled-coil complexes, with the largest increase in structure, binding and stability observed for peptides stapled close to the C-terminus with *ortho*-xylene. Binding strength is increased via a pre-organization mechanism, which consists of a large reduction of the unfavored entropic binding component, combined with a negative change in binding enthalpy. *Ortho*-, and *meta*-xylene crosslinkers resulted in similar coiled-coil binding strengths, although *ortho*-xylene reduced the effect of entropy the most. This effect was true for all three stapling sites and is due to the smaller size of the *ortho*-xylene crosslinker. Although there may be some dependence on amino acid composition, we conclude that *ortho*-xylene is the best crosslinker to stabilize helical peptides, despite *meta*-xylene being widely employed to date.

The effect of stapling on peptide-membrane partitioning was determined, and showed a two-fold difference between stapled peptide variants, although no direct correlation to location or staple type could be made. Lipopeptides of K_3GW-3*M* and K_3GW-3*O* were prepared via a novel on-resin stapling method. These peptides were tested in lipid-, and content-mixing experiments, and large increases in fusogenicity for the K3GW-3*O* variant were observed. K_3GW-3*M* also showed significantly increased content mixing, but exhibited a similar amount of lipid mixing to the parent peptide. We theorize that these differences in fusogenicity can be explained via reduced dissociation; increasing coiled-coil interactions without increasing lipid membrane interactions allows accumulation of more coiled-coil pairs at the fusion interface and therefore increases membrane fusion.

3.4 Experimental

Tentagel resin was purchased from Rapp Polymere. Dimethylformamide (DMF), piperidine, pyridine, acetic anhydride, trifluoroacetic acid (TFA) and acetonitrile (MeCN) were supplied from Biosolve. N,N-diisopropylethylamine (DIPEA) and Oxyma were purchased from Carl Roth. Dichloromethane (DCM) and diethyl ether were supplied by Honeywell. HBTU and all protected amino acids except Fmoc-Cys(mtt)-OH were purchased from Novabiochem. All other chemicals were

purchased from Sigma Aldrich. Ultrapure water was obtained from a MILLI-Q™ water purification system. Peptide concentration was established via absorption at 280 nm, determined using a CARY-300 UV-Vis spectrophotometer.

Peptide synthesis and purification All peptides were synthesized on solid phase using a CEM liberty blue automated, microwave-assisted, peptide synthesizer. Peptides were prepared on a 0.1 mmol scale using Tentagel HL RAM resin with a loading of 0.39 mmol/g. Fmoc deprotection was performed using 20% piperidine in DMF at 90˚C for 60 seconds. Amide coupling was achieved using 5 eq. of protected amino acid, 5 eq. DIC as activator and 5 eq. Oxyma as activator base, heated at 95 ˚C for 240 seconds. Acetylation of the peptide N-terminus after automated synthesis was performed using an excess of acetic anhydride and pyridine in DMF.

Lipidated peptides were made on resin via the coupling of 2.5 equivalents of N_3-PEG_4-COOH (see supplementary methods for synthesis details), with 2.5 eq of HBTU and 5 eq. of DIPEA in DMF for 2 hours at room temperature. After washing the resin with DMF, the azide was reduced using 10 eq. of PME_3 (1 M in toluene), with 4:1 dioxane:water as solvent for 2.5 hours. After the reaction was finished, the resin was washed thoroughly with 4:1 dioxane:water, MeOH and DMF. Lipidation was achieved using 2 eq. of cholesteryl hemisuccinate, 2 eq. of HBTU and 4 eq. of DIPEA in 1:1 DMF:DCM, and this lipidation step was performed twice to achieve complete conversion. After the final coupling the resin was washed with DMF, MeOH, and DCM, dried under vacuum, and the peptide was cleaved using a 92.5:2.5:2.5:2.5 mixture of TFA:TIPS:EDDT:water for 1 hour, after which the peptide was precipitated in cold diethyl ether, collected via centrifugation and lyophilized.

All peptides were purified by HPLC on a Shimadzu system consisting of two KC-20AR pumps and an SPD-20A or SPD-M20A detector equipped with a Kinetix Evo C18 column. Eluents consisted of 0.1% TFA in water (A) and 0.1% TFA in MeCN (B), with all peptides eluted using a gradient of 20-90% B over 35 minutes, with a flow rate of 12 mL/min. Collected fractions were checked for purity via LCMS, with the pure fractions being pooled and lyophilized. LC-MS spectra were recorded using a Thermo Scientific TSQ quantum access MAX mass detector connected to an Ultimate 3000 liquid chromatography system fitted with a 50x4.6 mm Phenomenex Gemini 3 μm C18 column.

Peptide stapling Intramolecular crosslinking was achieved by dissolving the peptide in a 1:1 mixture of MeCN:H_2O containing 10 mM NH_4HCO_3 up to a peptide

concentration of 500 µM. TCEP, 1 eq. was added as a 10 mM stock solution, and the reaction was stirred for 1 hour, followed by addition of 1.2 eq. of the dibromoxylene crosslinker (50 mM in DMF) and reacted for 3 hours. The reaction was quenched by the addition of 5% acetic acid, and purified using preparative HPLC. For the lipidated peptides, the crosslinking was performed on solid phase. In short; Cysteines protected with Mtt were incorporated into the peptide, and after automated synthesis these protecting groups were removed by incubating the resin with 2% TFA, and 3% TIS in DCM for 2 minutes, followed by washing the resin with DCM twice. This was repeated until no more color appeared when a small amount of the resin was mixed with TFA. Crosslinking was achieved by addition of 1.5 eq. of the crosslinker and 2.5 eq. of DIPEA in 1:1 DMF:TFE, and incubating this reaction for 3 hours. On resin stapling was usually performed before lipidation.

Circular dichroism measurements. CD spectra were recorded on a JASCO J-815 CD spectrometer fitted with a Peltier temperature controller. Unless otherwise specified, samples were measured at 20 ˚C in a quartz cuvette with a 2 mm path length. Spectra were recorded from 190 to 260 nm at 1 nm intervals, with a bandwidth of 1 nm, with the final spectrum consisting of the average of 5 sequentially recorded spectra. The mean residue molar ellipticity (θ, deg cm^2 $dmol.res^{-1}$) was calculated according to equation 1:

$$[\theta] = (100 * [\theta]_{obs})/(c * n * l) \qquad (1)$$

With $[\theta]_{obs}$ representing the observed ellipticity in mdeg, c the peptide concentration in mM, n the number of peptide bonds and l the path length of the cuvette in cm. The fraction of α-helical peptide could be calculated from the MRE using equation 2:

$$F_{helix} = ([\theta]_{222} - [\theta]_0)/([\theta]_{max} - [\theta]_0) \qquad (2)$$

With the maximum theoretical mean residue ellipticity, $[\theta]_{max}$, defined as $[\theta]_{max} = [\vartheta]_\infty (n - x)/n$ for a helix with *n* residues and *x* a number of amino acids assumed not to participate in helix formation (in this case 3). $[\theta]_\infty$ is defined as the theoretical helicity of an infinite α-helix and is temperature dependent, defined via $[\theta]_\infty = (-44000 + 250T)$, with *T* being the temperature in °C. The minimal expected absorbance at 222 nm for a random coil is defined in $[\theta]_0$, which is also temperature dependent via the relationship $[\theta]_0 = 2220 - 53T$.

Tryptophan fluorescence titration. Fluorescence was measured in 96 well plates using a TECAN Infinite M1000 Pro microplate reader. Liposomes of the composition 2:1:1 DOPC:DOPE:Cholesterol were prepared at a 10 mM concentration via extrusion in PBS buffer, using an Avanti mini extruder with 100 nm polycarbonate membranes. Titration series of liposomes in PBS buffer were prepared with concentrations between 25 and 3750 μM, with the peptide concentration held constant at 2.5 μM. Samples were prepared in 96 well plates, and after 60 minutes of incubation a fluorescence spectrum was taken between 300 and 450 nm. The maximum fluorescence of each sample was plotted as a fold increase of the fluorescence of the peptide without liposomes present, and fitted against equation 3 to determine the partition constant:

$$F = 1 + (F_{max} - 1) * \left(K_p * X\right)/(55.3 + K_p * X) \qquad (3)$$

Where the normalized fluorescence, *F*, is dependent on the maximum fluorescence when all peptide is bound to the membrane F_{max}, molar partition coefficient K_p, the lipid concentration *X* and the concentration of water which is assumed to be constant at 55.3 M. Experimental data of 3 separate experiments was fitted to equation 3 using the least-squares method to yield the partition coefficient, and the standard error of fitting.

Isothermal titration calorimetry. ITC measurements were performed on a Malvern MicroCal PEAQ-ITC automated calorimeter. In a standard experiment, the measurement cell contained 200 μL of 10 μM peptide K and the syringe was filled with E_3GY at 100 μM concentration, with both peptides dissolved in PBS. The syringe content was added in 21 injections of 1.9 μL at 120s intervals, except the first injection which was 0.5 μL. The reference power was set at 2.0 μCal/sec, and experiments were performed at 25 ˚C. The data was analyzed with the Microcal PEAQ-ITC analysis software, and fitted to a single binding site model to generate the thermodynamic binding parameters. The experiment was repeated on 3 separate occasions, and the experimental results with the lowest reduced chi-squared value are represented in this paper.

Lipid and content mixing experiments Liposomes with the lipid composition 2:1:1 DOPC:DOPE:Cholesterol were used at a 500 μM concentration, where 1% of the lipids was substituted with the respective lipopeptide. Lipid films were prepared via evaporation of lipid and lipopeptide stock solutions in 1:1 $CHCl_3$:MeOH under a stream of nitrogen, followed by high vacuum for at least 2 hours. The lipid films

were rehydrated via vortex mixing with PBS buffer and sonication for 5 minutes at 55˚C in a Branson 2510 bath sonicator. The liposomes were checked for size and polydispersity (PDI) via DLS (Malvern Zetaszier Nano S), and sonicated for a second time if the PDI was larger than 0.25. Lipid mixing was assayed via the incorporation of 0.5% DOPE-NBD (1,2-dioleoyl-sn-glycero-3-phosphoethanolamine-N-(7-nitro-2-1,3-benzoxadiazol-4-yl)) and 0.5% DOPE-LR (1,2-dioleoyl-sn-glycero-3-phosphoethanolamine-N-(lissamine rhodamine B sulfonyl)) in the lipid membranes of the CPK-containing liposomes. 100 µL of fluorescent CPK-containing liposomes were mixed with 100 µL of non-fluorescent CPE-decorated liposomes, and the emission of NBD at 530 nm was followed over time. Each experiment included a positive control consisting of liposomes at a 500 µM concentration and 0.25% of both DOPE-LR and DOPE-NBD, and a negative control where the fluorescent liposomes were combined with liposomes without CPE. The standard deviation was calculated on the average of 4 separate measurement samples, and the experiment was repeated at least 3 times.

Content mixing was assayed via the incorporation of 10 mM Sulforhodamine B in the hydration buffer of CPE-decorated liposomes. After sonication, the unincorporated rhodamine was removed using an Illustra NAP-25 size-exclusion column. For each experiment, 100 µL of sulforhodamine-containing CPE-liposomes were mixed with 100 µL CPK-containing liposomes, and the fluorescence of sulforhodamine followed over time at 585 nm. The value was normalized via referencing a positive control consisting of liposomes containing 5 mM sulforhodamine B prepared in the same manner and a negative control where the fluorescent CPE liposomes were combined with plain liposomes. The standard deviation was calculated on the average of 4 separate measurement samples, and the experiment was repeated at least 3 times.

Change in fluorescence was measured in 96 well plates using a TECAN Infinite M1000 Pro microplate reader. The percentage of lipid and content mixing was calculated using the following formula (Equation 4):

$$\%\, mixing = (F_t - F_0)/(F_{max} - F_0) \qquad (4)$$

Where F_t is the fluorescence at time t, and F_0 and F_{max} are the fluorescence of the negative and positive controls at the same time point. Processing of fluorescence data and one-way ANOVA analysis was performed in GraphPad Prism 8.1.1.

3.5 Acknowledgements

I gratefully acknowledge Professor Nathaniel I. Martin and Ioli Kotsogianni from the Institute of Biology (IBL) at Leiden University for access to, and technical assistance with, the ITC measurements.

3.6 References

1. Pelay-Gimeno, M.*, et al.* (**2015**) Structure-Based Design of Inhibitors of Protein-Protein Interactions: Mimicking Peptide Binding Epitopes. *Angew. Chem. Int. Edit. 54*, 8896-8927.

2. Klein, M. (**2017**) Stabilized helical peptides: overview of the technologies and its impact on drug discovery. *Expert Opin. Drug. Dis. 12*, 1117-1125.

3. Hill, T. A.*, et al.* (**2014**) Constraining Cyclic Peptides To Mimic Protein Structure Motifs. *Angew. Chem. Int. Edit. 53*, 13020-13041.

4. Siegert, T. R.*, et al.* (**2016**) Analysis of Loops that Mediate Protein-Protein Interactions and Translation into Submicromolar Inhibitors. *J. Am. Chem. Soc. 138*, 12876-12884.

5. Nilsson, A., Lindgren, J., and Karlstrom, A. E. (**2017**) Intramolecular Thioether Crosslinking to Increase the Proteolytic Stability of Affibody Molecules. *Chembiochem : a European journal of chemical biology 18*, 2056-2062.

6. Walensky, L. D.*, et al.* (**2004**) Activation of apoptosis in vivo by a hydrocarbon-stapled BH3 helix. *Science 305*, 1466-1470.

7. Walensky, L. D., and Bird, G. H. (**2014**) Hydrocarbon-Stapled Peptides: Principles, Practice, and Progress. *J. Am. Chem. Soc. 57*, 6275-6288.

8. Wang, C.*, et al.* (**2018**) Discovery of Hydrocarbon-Stapled Short alpha-Helical Peptides as Promising Middle East Respiratory Syndrome Coronavirus (MERS-CoV) Fusion Inhibitors. *J. Med. Chem. 61*, 2018-2026.

9. Carvajal, L. A.*, et al.* (**2018**) Dual inhibition of MDMX and MDM2 as a therapeutic strategy in leukemia. *Sci. Transl. Med. 10*.

10. Cromm, P. M., Spiegel, J., and Grossmann, T. N. (**2015**) Hydrocarbon Stapled Peptides as Modulators of Biological Function. *ACS Chem. Biol. 10*, 1362-1375.

11. Gongora-Benitez, M., Tulla-Puche, J., and Albericio, F. (**2014**) Multifaceted Roles of Disulfide Bonds. Peptides as Therapeutics. *Chem. Rev. 114*, 901-926.

12. Shepherd, N. E.*, et al.* (**2006**) Modular alpha-helical mimetics with antiviral activity against respiratory syncitial virus. *J. Am. Chem. Soc. 128*, 13284-13289.

13. Khoo, K. K.*, et al.* (**2011**) Lactam-Stabilized Helical Analogues of the Analgesic mu-Conotoxin KIIIA. *J. Med. Chem. 54*, 7558-7566.

14. Kawamoto, S. A.*, et al.* (**2012**) Design of Triazole-Stapled BCL9 α-Helical Peptides to Target the β-Catenin/B-Cell CLL/lymphoma 9 (BCL9) Protein–Protein Interaction. *J. Med. Chem. 55*, 1137-1146.

15. Wu, Y. T.*, et al.* (**2017**) Targeting the Genome-Stability Hub Ctf4 by Stapled-Peptide Design. *Angew. Chem. Int. Edit. 56*, 12866-12872.

16. Peraro, L.*, et al.* (**2017**) Diversity-Oriented Stapling Yields Intrinsically Cell-Penetrant Inducers of Autophagy. *J. Am. Chem. Soc. 139*, 7792-7802.

17. Fairlie, D. P., and Dantas de Araujo, A. (**2016**) Stapling peptides using cysteine crosslinking. *Peptide Science 106*, 843-852.

18. de Araujo, A. D.*, et al.* (**2014**) Comparative alpha-Helicity of Cyclic Pentapeptides in Water. *Angew. Chem. Int. Edit. 53*, 6965-6969.

19. Tian, Y.*, et al.* (**2017**) Effect of Stapling Architecture on Physiochemical Properties and Cell Permeability of Stapled alpha-Helical Peptides: A Comparative Study. *Chembiochem : a European journal of chemical biology 18*, 2087-2093.

20. Lau, Y. H.*, et al.* (**2015**) Peptide stapling techniques based on different macrocyclisation chemistries. *Chem. Soc. Rev. 44*, 91-102.

21. Henchey, L. K., Jochim, A. L., and Arora, P. S. (**2008**) Contemporary strategies for the stabilization of peptides in the alpha-helical conformation. *Curr. Opin. Chem. Biol. 12*, 692-697.

22. Rao, T.*, et al.* (**2013**) Truncated and Helix-Constrained Peptides with High Affinity and Specificity for the cFos Coiled-Coil of AP-1. *Plos One 8*.

23. Haney, C. M., and Horne, W. S. (**2013**) Oxime Side-Chain Cross-Links in an -Helical Coiled-Coil Protein: Structure, Thermodynamics, and Folding-Templated Synthesis of Bicyclic Species. *Chem. Eur. J. 19*, 11342-11351.

24. Lathbridget, A., and Mason, J. M. (**2019**) Combining Constrained Heptapeptide Cassettes with Computational Design To Create Coiled-Coil Targeting Helical Peptides. *ACS Chem. Biol. 14*, 1293-1304.

25. Robson Marsden, H.*, et al.* (**2013**) Controlled liposome fusion mediated by SNARE protein mimics. *Biomat. Sci. 1*, 1046-1054.

26. Jo, H.*, et al.* (**2012**) Development of alpha-Helical Calpain Probes by Mimicking a Natural Protein-Protein Interaction. *J. Am. Chem. Soc. 134*, 17704-17713.

27. Acharyya, A.*, et al.* (**2019**) Exposing the Nucleation Site in alpha-Helix Folding: A Joint Experimental and Simulation Study. *J. Phys. Chem. B 123*, 1797-1807.

28. Wu, H. F.*, et al.* (**2018**) Design of a Short Thermally Stable -Helix Embedded in a Macrocycle. *Chembiochem : a European journal of chemical biology 19*, 902-906.

29. Iqbal, E. S.*, et al.* (**2019**) A new strategy for the in vitro selection of stapled peptide inhibitors by mRNA display. *Chem. Commun. 55*, 8959-8962.

30. Diderich, P.*, et al.* (**2016**) Phage Selection of Chemically Stabilized alpha-Helical Peptide Ligands. *ACS Chem. Biol. 11*, 1422-1427.

31. Sudhof, T. C., and Rothman, J. E. (**2009**) Membrane Fusion: Grappling with SNARE and SM Proteins. *Science 323*, 474-477.

32. Marsden, H. R.*, et al.* (**2009**) A Reduced SNARE Model for Membrane Fusion. *Angew. Chem. Int. Edit. 48*, 2330-2333.

33. Marsden, H. R., Tomatsu, I., and Kros, A. (**2011**) Model systems for membrane fusion. *Chem. Soc. Rev. 40*, 1572-1585.

34. Koukalova, A*., et al.* (**2018**) Distinct roles of SNARE-mimicking lipopeptides during initial steps of membrane fusion. *Nanoscale 10*, 19064-19073.

35. Rabe, M., Zope, H. R., and Kros, A. (**2015**) Interplay between Lipid Interaction and Homo-coiling of Membrane-Tethered Coiled-Coil Peptides. *Langmuir 31*, 9953-9964.

36. Litowski, J. R., and Hodges, R. S. (**2002**) Designing heterodimeric two-stranded alpha-helical coiled-coils - Effects of hydrophobicity and alpha-helical propensity on protein folding, stability, and specificity. *J. Biol. Chem. 277*, 37272-37279.

37. Green, B. R*., et al.* (**2013**) Cyclic analogs of galanin and neuropeptide Y by hydrocarbon stapling. *Bioorgan. Med. Chem. 21*, 303-310.

38. Pierce, M. M., Raman, C. S., and Nall, B. T. (**1999**) Isothermal titration calorimetry of protein-protein interactions. *Meth. Enzymol. 19*, 213-221.

39. Miles, J. A*., et al.* (**2016**) Hydrocarbon constrained peptides - understanding preorganisation and binding affinity. *Chem. Sci. 7*, 3694-3702.

40. Lindhout, D. A*., et al.* (**2004**) NMR solution structure of a highly stable de novo heterodimeric coiled-coil. *Biopolymers 75*, 367-375.

41. Rabe, M*., et al.* (**2016**) A Coiled-Coil Peptide Shaping Lipid Bilayers upon Fusion. *Biophys. J. 111*, 2162-2175.

42. Pluhackova, K*., et al.* (**2015**) Spontaneous Adsorption of Coiled-Coil Model Peptides K and E to a Mixed Lipid Bilayer. *J. Phys. Chem. B. 119*, 4396-4408.

43. Versluis, F*., et al.* (**2013**) In Situ Modification of Plain Liposomes with Lipidated Coiled Coil Forming Peptides Induces Membrane Fusion. *J. Am. Chem. Soc. 135*, 8057-8062.

44. Bosshard, H. R*., et al.* (**2001**) Energetics of coiled coil folding: The nature of the transition states. *Biochem. 40*, 3544-3552.

45. McDargh, Z. A., Polley, A., and O'Shaughnessy, B. (**2018**) SNARE-mediated membrane fusion is a two-stage process driven by entropic forces. *FEBS letters 592*, 3504-3515.

46. Mostafavi, H*., et al.* (**2017**) Entropic forces drive self-organization and membrane fusion by SNARE proteins. *P. Natl. Acad. Sci. USA 114*, 5455-5460.

Supporting Information for Chapter 3

Circular Dichroism

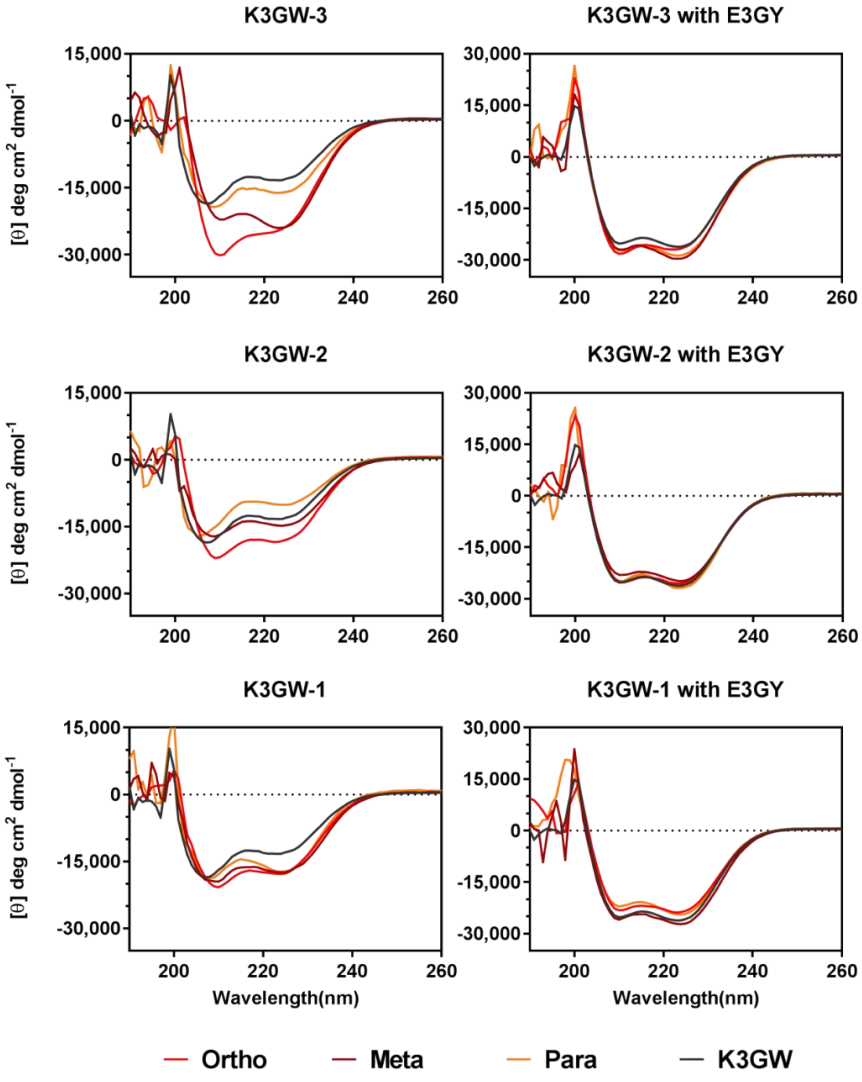

Figure S3.1: CD spectra of xylene stapled peptide variants by themselves (left) and in combination with E_3GY (right). Peptides were dissolved at a total concentration of 50 µM in PBS at pH 7.4, and spectra were measured at 20˚C.

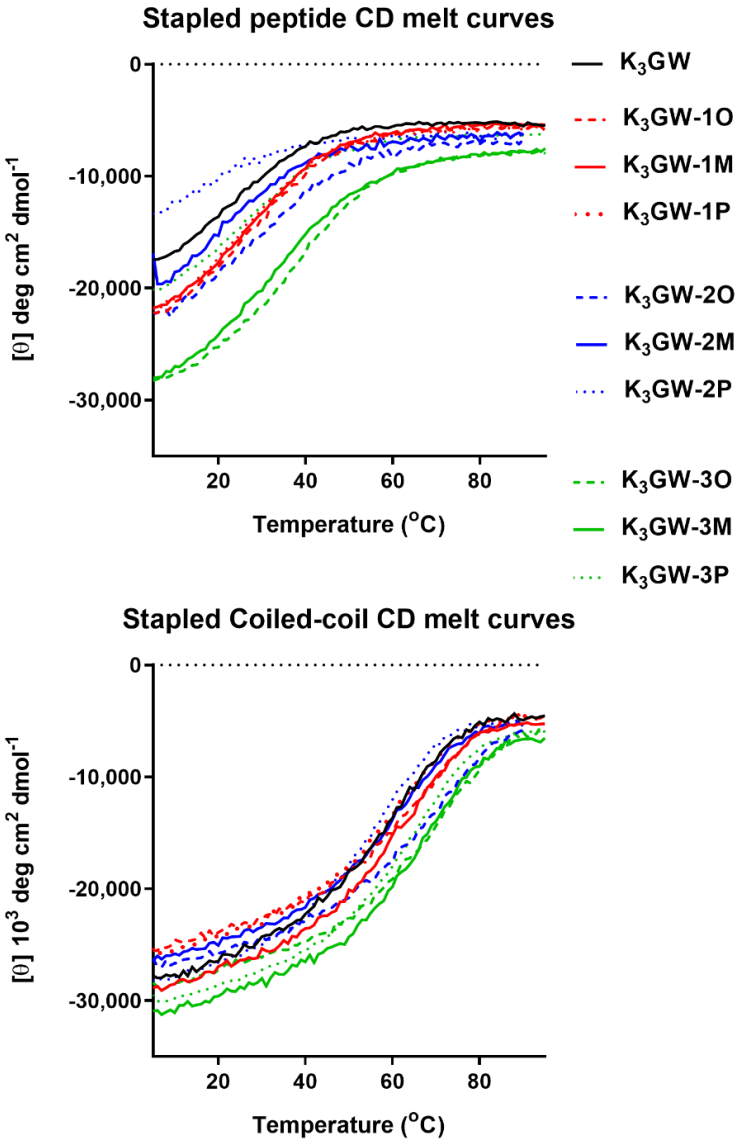

Figure S3.2: CD melting curves of stapled peptide variants (top) and their respective coiled coils with peptide E_3GY (bottom). Melting curves were measured from 5 °C to 95 °C at a total peptide concentration of 50 µM.

Table S3.1: CD spectroscopy results for peptide K_3GW and its stapled derivatives.

Peptide	$[\Theta]_{222nm}$ (deg cm^2 dmol^{-1})	$[\Theta]_{222nm}/[\Theta]_{208nm}$	Helicity (%)	Tm (°C)
K_3GW	-13247	0.72	41%	22
K_3GW-1O	-17662	0.89	54%	27
K_3GW-1M	-17255	0.89	53%	28
K_3GW-1P	-16898	0.90	51%	24
K_3GW-2O	-18408	0.86	56%	30
K_3GW-2M	-14607	0.85	45%	20
K_3GW-2P	-9949	0.63	32%	16
K_3GW-3O	-24980	0.89	75%	39
K_3GW-3M	-23790	1.18	71%	32
K_3GW-3P	-16109	0.84	49%	26

Table S3.2: Measured characteristics of peptide K_3GW and its stapled variants as a coiled coil with peptide E_3GY, determined via CD spectroscopy.

Peptide	$[\Theta]_{222nm}$ (deg cm^2 dmol^{-1})	$[\Theta]_{222nm}/[\Theta]_{208nm}$	Helicity (%)	T_m (°C)
K_3GW	-26080	1.13	78%	60
K_3GW-1O	-23722	1.13	71%	65
K_3GW-1M	-26946	1.13	80%	63
K_3GW-1P	-24179	1.19	72%	61
K_3GW-2O	-25466	1.13	76%	69
K_3GW-2M	-24500	1.16	73%	62
K_3GW-2P	-26712	1.17	79%	58
K_3GW-3O	-27006	1.04	80%	72
K_3GW-3M	-29608	1.22	88%	68
K_3GW-3P	-28577	1.14	85%	65

Isothermal Titration Calorimetry

Table S3.3: Binding thermodynamics of peptide K_3GW and its stapled variants as a coiled coil with peptide E_3GY, determined via isothermal titration calorimetry .

Peptide	N sites	K_d (nM)	ΔH (kJ/mol)	ΔG (kJ/mol)	-TΔS (kJ/mol)	R. Chi-Sqr. (kcal/mol)²
K_3GW	0.98	73.1 +/- 9.0	-77.3 +/- 1.1	-40.7	36.7	0.11
K_3GW-1O	0.78	59 +/- 11.5	-73.6 +/- 1.4	-41.2	32.3	0.21
K_3GW-1M	0.83	54.1 +/- 7.4	-76.9 +/- 1.0	-41.5	35.5	0.11
K_3GW-2O	0.80	53.9 +/- 7.5	-76.5 +/- 1.0	-41.5	35.1	0.12
K_3GW-2M	0.83	48.1 +/- 6.4	-81.9 +/- 1.0	-41.8	40.3	0.12
K_3GW-3O	0.87	22.7 +/- 5.7	-67.7 +/- 1.2	-43.5	24.1	0.20
K_3GW-3M	0.92	24.1 +/- 5.1	-72.7 +/- 1.2	-43.5	29.2	0.20
K_3GW-3P	0.92	51.4 +/- 5.0	-74.0 +/- 0.7	-41.6	32.6	0.06

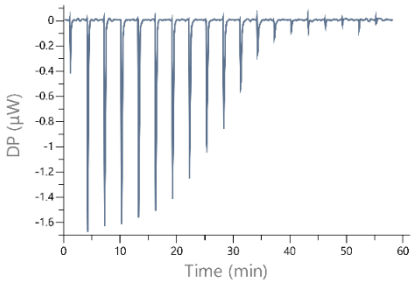
DP (µW)
Time (min)

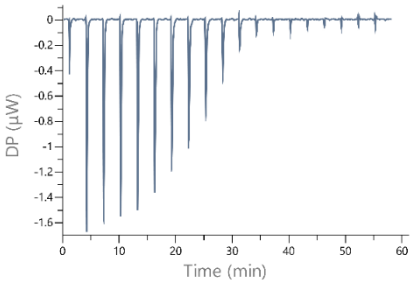
DP (µW)
Time (min)

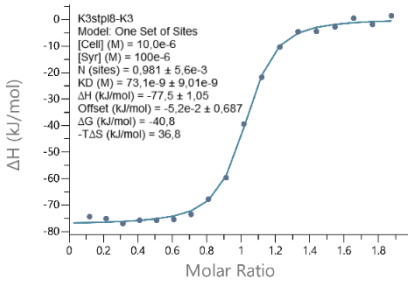
K3stpl8-K3
Model: One Set of Sites
[Cell] (M) = 10,0e-6
[Syr] (M) = 100e-6
N (sites) = 0,981 ± 5,6e-3
KD (M) = 73,1e-9 ± 9,01e-9
ΔH (kJ/mol) = -77,5 ± 1,05
Offset (kJ/mol) = -5,2e-2 ± 0,687
ΔG (kJ/mol) = -40,8
-TΔS (kJ/mol) = 36,8
ΔH (kJ/mol)
Molar Ratio

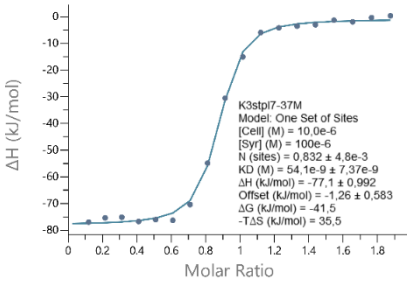
K3stpl7-37M
Model: One Set of Sites
[Cell] (M) = 10,0e-6
[Syr] (M) = 100e-6
N (sites) = 0,832 ± 4,8e-3
KD (M) = 54,1e-9 ± 7,37e-9
ΔH (kJ/mol) = -77,1 ± 0,992
Offset (kJ/mol) = -1,26 ± 0,583
ΔG (kJ/mol) = -41,5
-TΔS (kJ/mol) = 35,5
ΔH (kJ/mol)
Molar Ratio

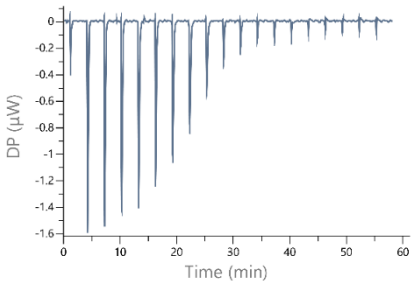
DP (µW)
Time (min)

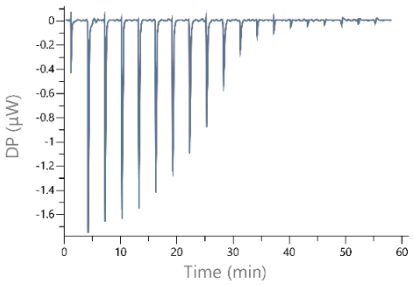
DP (µW)
Time (min)

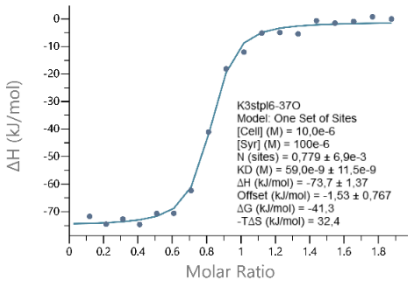
K3stpl6-37O
Model: One Set of Sites
[Cell] (M) = 10,0e-6
[Syr] (M) = 100e-6
N (sites) = 0,779 ± 6,9e-3
KD (M) = 59,0e-9 ± 11,5e-9
ΔH (kJ/mol) = -73,7 ± 1,37
Offset (kJ/mol) = -1,53 ± 0,767
ΔG (kJ/mol) = -41,3
-TΔS (kJ/mol) = 32,4
ΔH (kJ/mol)
Molar Ratio

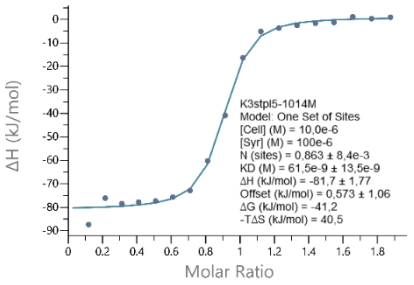
K3stpl5-1014M
Model: One Set of Sites
[Cell] (M) = 10,0e-6
[Syr] (M) = 100e-6
N (sites) = 0,863 ± 8,4e-3
KD (M) = 61,5e-9 ± 13,5e-9
ΔH (kJ/mol) = -81,7 ± 1,77
Offset (kJ/mol) = 0,573 ± 1,06
ΔG (kJ/mol) = -41,2
-TΔS (kJ/mol) = 40,5
ΔH (kJ/mol)
Molar Ratio

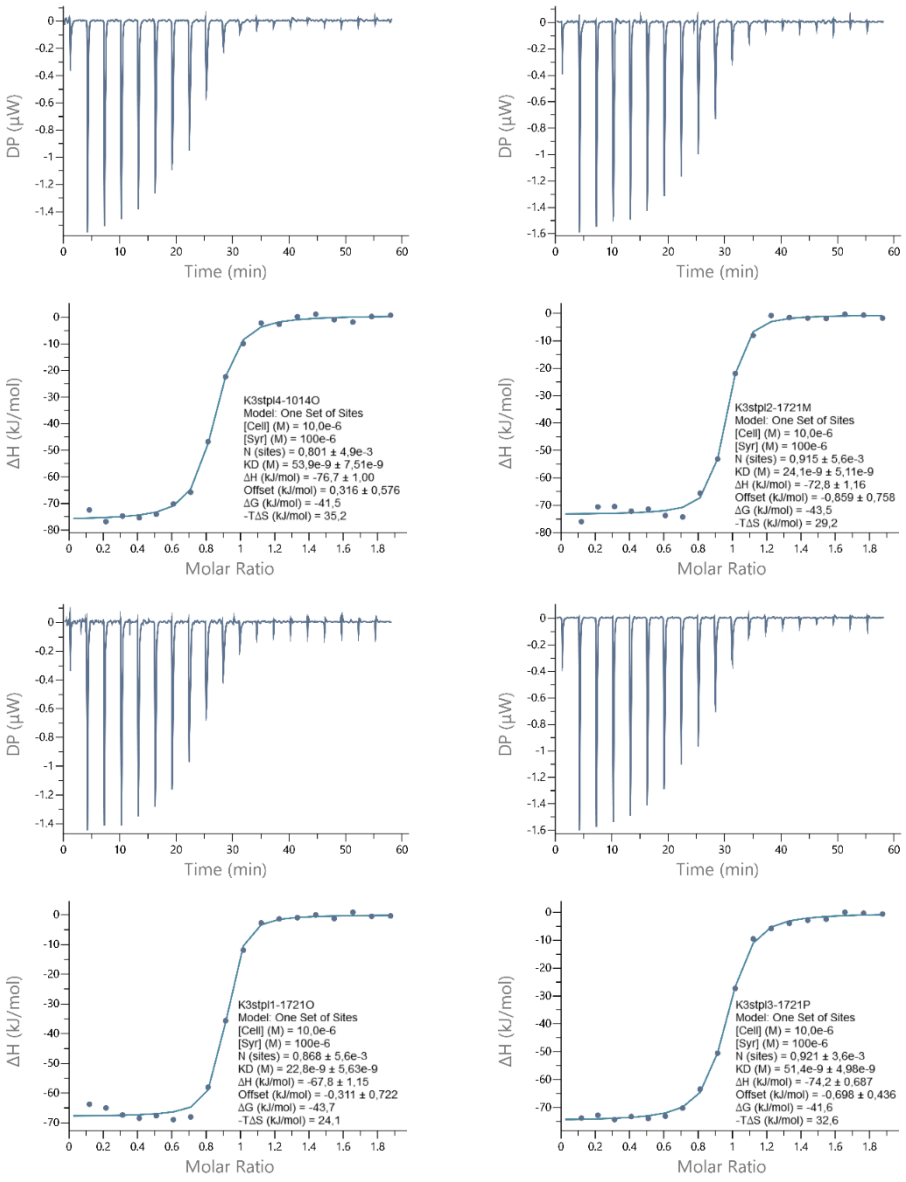

Figure S3.3: ITC binding curves of K_3GW and stapled variants with binding partner E_3GY.

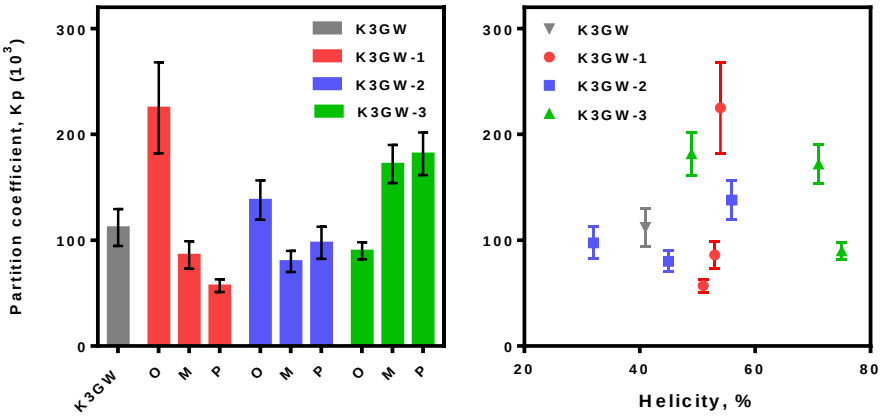

Figure S3.4: Overview of the membrane partition coefficient of stapled peptide variants (left) and membrane partition set against peptide helicity (right) as determined via CD spectroscopy. Error bars represent the standard error of fitting.

Table S3.4: Membrane binding affinity determined via tryptophan fluorescence for peptide K_3GW and its stapled derivatives. The shown values are derived from the fitted curves shown in Figure S3.5.

Peptide	K_p (10^3)	R^2	ΔG (KJ/Mol)	ΔΔG (KJ/Mol)
K_3GW	112	0.93	-28.80	-
K_3GW-1O	225	0.88	-30.53	-1.73
K_3GW-1M	86	0.96	-28.15	0.65
K_3GW-1P	57	0.98	-27.13	1.67
K_3GW-2O	137.8	0.96	-29.32	-0.51
K_3GW-2M	80	0.96	-27.97	0.83
K_3GW-2P	97.5	0.95	-28.46	0.34
K_3GW-3O	90	0.98	-28.26	0.54
K_3GW-3M	172	0.97	-29.87	-1.06
K_3GW-3P	181.7	0.97	-30.00	-1.20

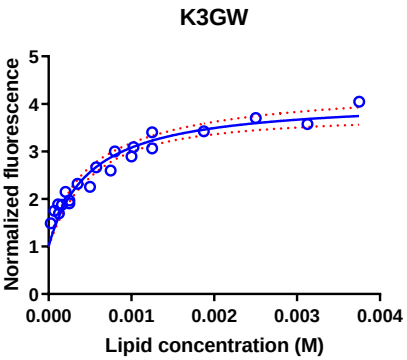
K3GW
Normalized fluorescence
Lipid concentration (M)
0
1
2
3
4
5
0.000
0.001
0.002
0.003
0.004

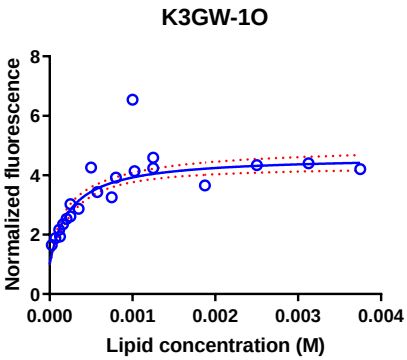
K3GW-1O
Normalized fluorescence
Lipid concentration (M)
0
2
4
6
8
0.000
0.001
0.002
0.003
0.004

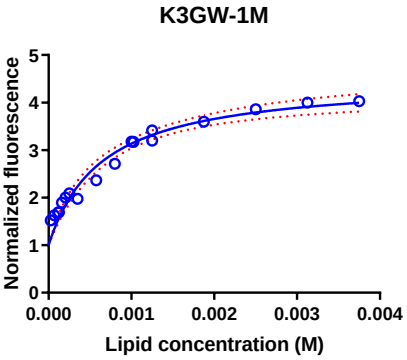
K3GW-1M
Normalized fluorescence
Lipid concentration (M)
0
1
2
3
4
5
0.000
0.001
0.002
0.003
0.004

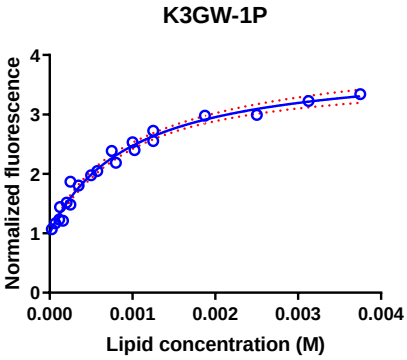
K3GW-1P
Normalized fluorescence
Lipid concentration (M)
0
1
2
3
4
0.000
0.001
0.002
0.003
0.004

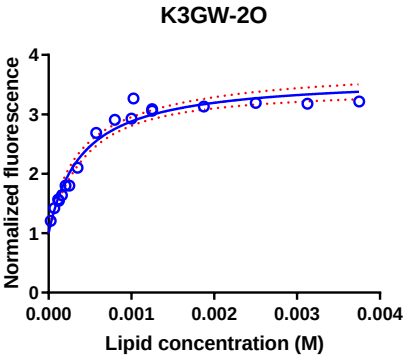
K3GW-2O
Normalized fluorescence
Lipid concentration (M)
0
1
2
3
4
0.000
0.001
0.002
0.003
0.004

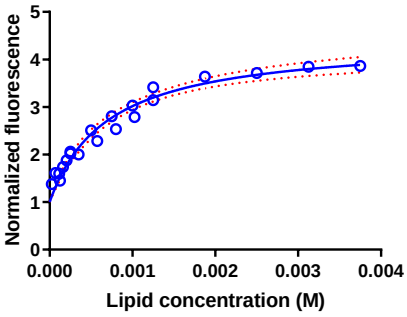
K3GW-2M
Normalized fluorescence
Lipid concentration (M)
0
1
2
3
4
5
0.000
0.001
0.002
0.003
0.004

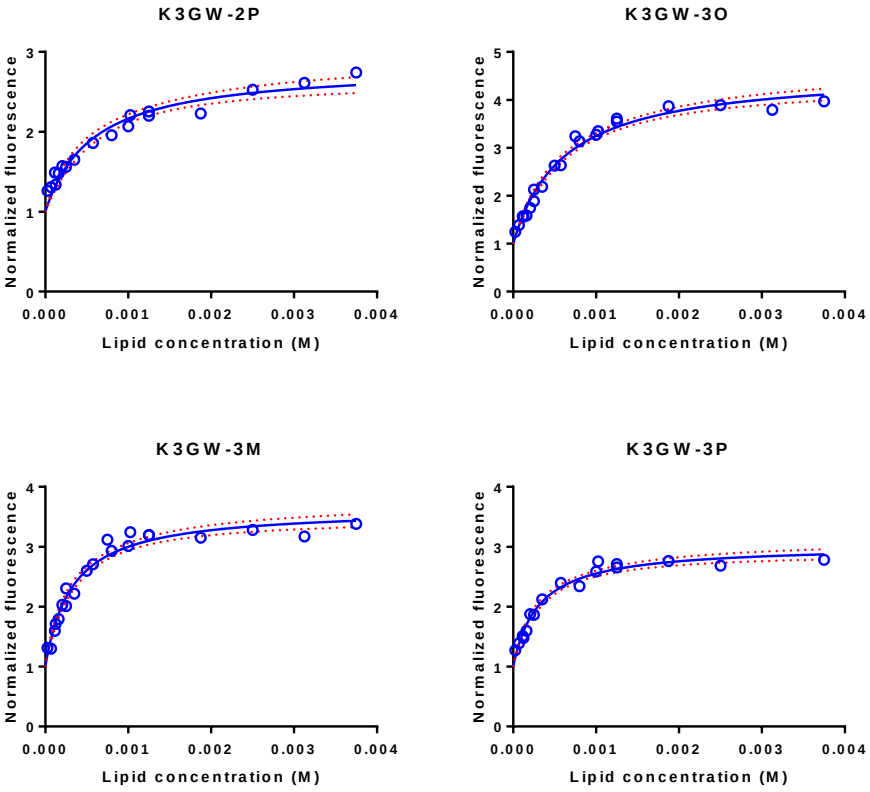

Figure S3.5: Fitting curves used to determine the membrane partition coefficient (Kp) of the stapled peptides. Red dotted lines represent the 95% confidence interval of the fit.

CD spectra with liposomes

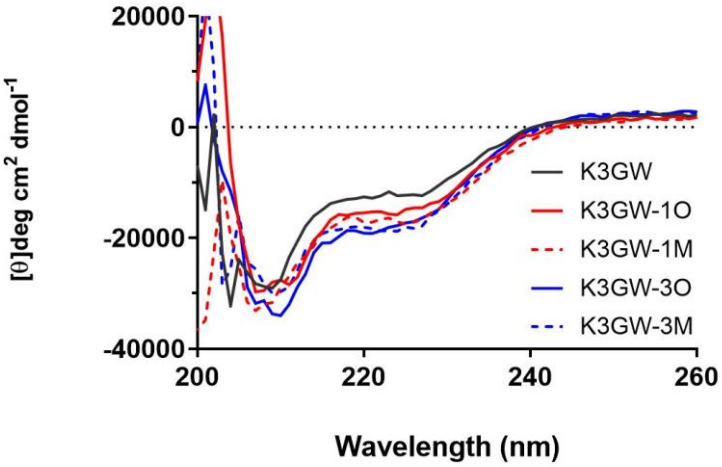

Figure S3.6: CD spectra of stapled peptides when combined with liposomes. Peptide concentration is 10 µM, liposomes are at a 1 mM lipid concentration and consist of DOPC:DOPE:Cholesterol in a 2:1:1 ratio. All spectra were measured in PBS in a 10 mm quartz cuvette at 25˚C.

Lipidated peptide structures

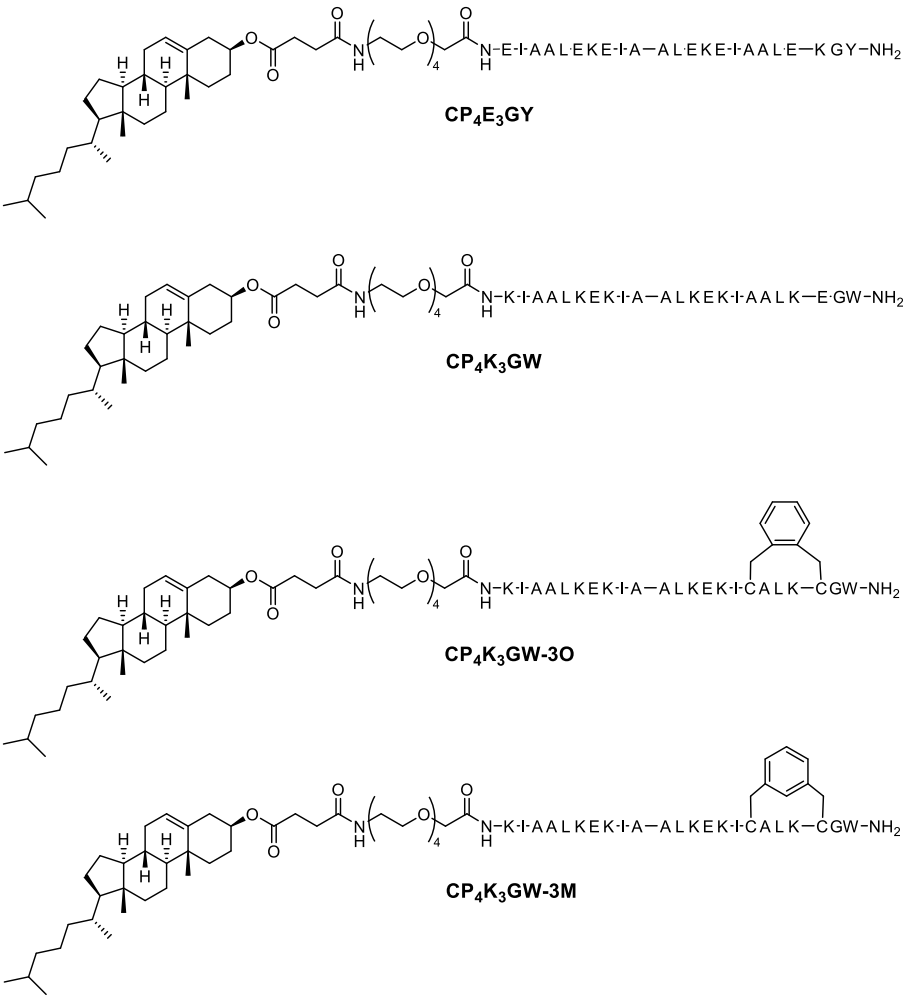

Scheme S3.1: Structures of lipidated peptides used for membrane fusion studies in this manuscript.

Lipid and content mixing control experiments

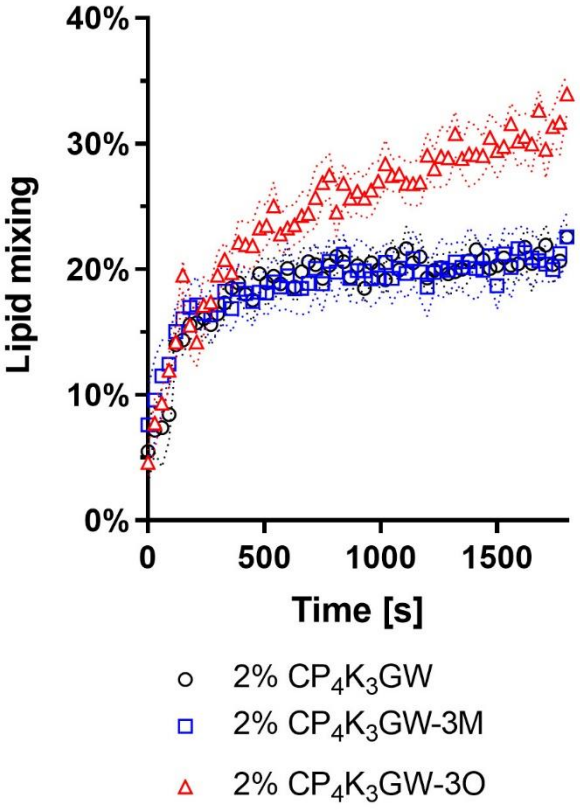

Figure S3.7: Lipid mixing experiments performed with 2% lipopeptides in the liposomal membranes. Graphs show the change in mixing over time, and the standard deviation between 4 samples followed simultaneously. Experiments were performed at 500 μM total lipid concentration in pH 7.4 PBS at 20˚C. Observed fluorescence was normalized against 0% and 100% control samples.

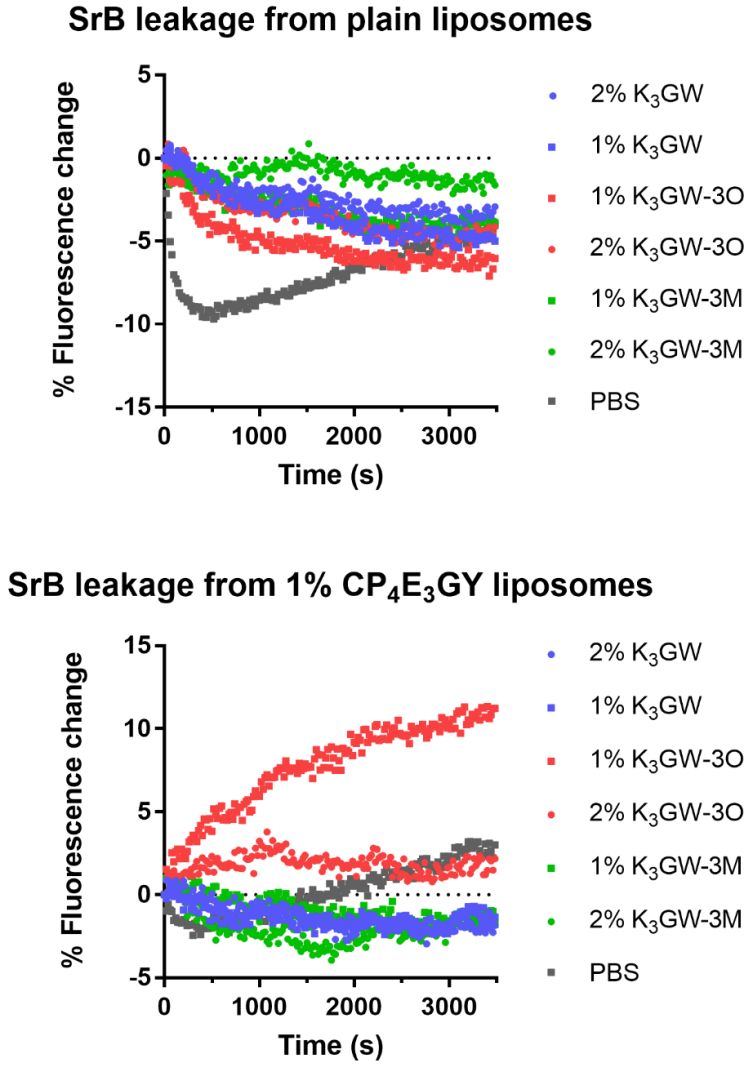

Figure S3.8: Sulforhodamine B leakage experiments for stapled peptide variants. Liposomes (500 μM lipid concentration) filled with sulforhodamine B were combined with acylated variants of peptide K_3GW at concentrations similar to those used in content mixing experiments, and change in absolute fluorescence was observed over time. No peptide was added to the samples labelled 'PBS'.

Homodimerization of stapled peptides

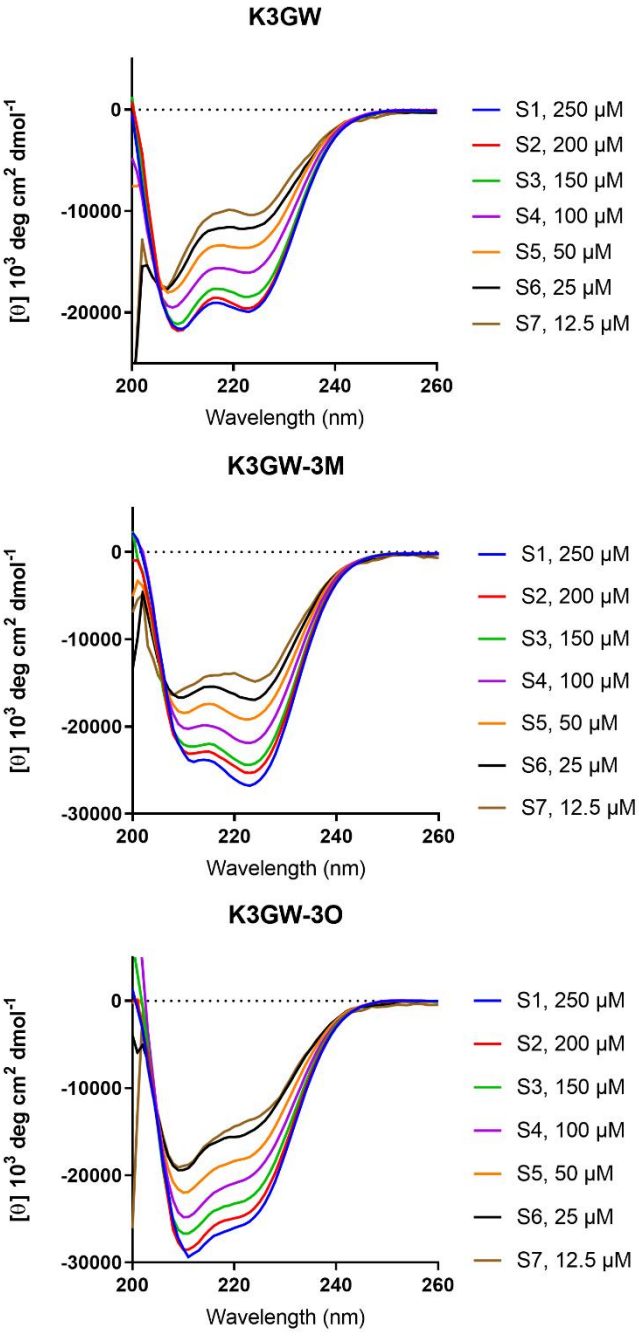

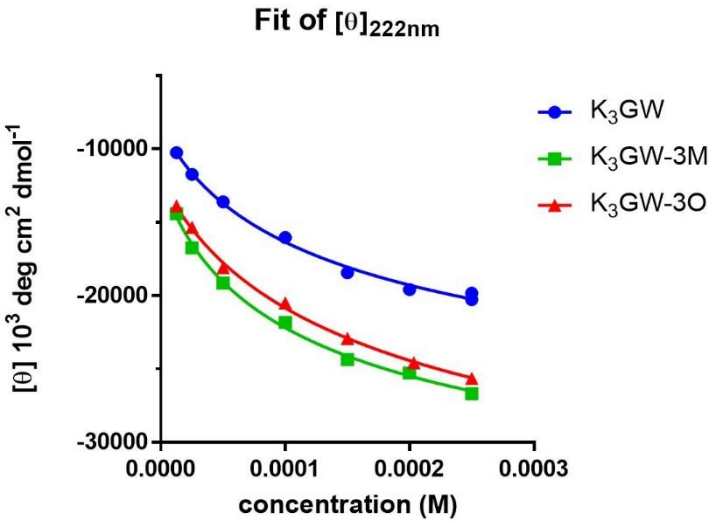

Figure S3.9: CD titration of peptide K_3GW, K_3GW-*3M*, and K_3GW-*3O* to determine homodimer formation of these peptide (top), and the extrapolated absorbance at 222 nm plotted against the concentration (bottom). Spectra were recorded at 25˚C in PBS buffer.

Table S3.5: Results of a non-linear fit of the CD ellipticity data shown in Figure S3.9 to determine the peptide affinity constant (K_a) of homodimer formation. $[\theta]_m$ and $[\theta]_d$ are fitted constants and represent the CD ellipticity values of the peptide as a monomer and a dimer respectively.

Peptide	$[\theta]_m$ 10^3 deg cm^2 dmol^{-1}	$[\theta]_d$ 10^3 deg cm^2 dmol^{-1}	K_a (10^3)	R^2
K3GW	-8434	-33396	3.41	0.995
K3GW-3O	-12010	-39808	4.57	0.997
K3GW-3M	-12056	-43076	2.76	0.998

Fitting procedure for homodimer formation

To calculate the peptide homodimerization from the CD spectra, the following chemical equilibria and equations are employed:

$$2P_m \leftrightarrow P_d \quad \text{(S1)}$$

$$K_d = \frac{[P_m]^2}{[P_d]} \quad \text{(S2)}$$

$$[P_t] = [P_m] + 2[P_d] \quad \text{(S3)}$$

where P_m and P_d represent the monomer and dimer concentration, and P_t the total peptide concentration.

From this Equation S4 can be derived:

$$[P_d] = \frac{[P_m]^2}{K_d} \qquad [P_t] = [P_m] + \frac{2[P_m]^2}{K_d} \quad \text{(S4)}$$

And a solution for P_m is shown as Equation S5:

$$[P_m] = \frac{K_d}{4}\left(-1 + \sqrt{1 + \frac{8[P_t]}{K_d}}\right) \quad \text{(S5)}$$

The equation for the measured absorbance θ as a function of the absorbance of the peptide as a monomer (θ_m) and dimer (θ_d), which are constants, is as follows:

$$\theta = \frac{[P_m][\theta_m] + 2[P_d][\theta_d]}{[P_t]} \quad \text{(S6)}$$

Combining S6 with S4 gives us the following:

$$\theta = \frac{[P_m][\theta_m] + \frac{2[P_m]^2}{K_d}[\theta_d]}{[P_t]} \quad \text{(S7)}$$

Using this equation combined with the equation above for P_m, the binding curve of the peptides can be fitted.

Synthesis of N_3-PEG_4-COOH

The synthetic route to produce the polyethylene glycol crosslinker used in the preparation of lipopeptides is shown in scheme S3.2.

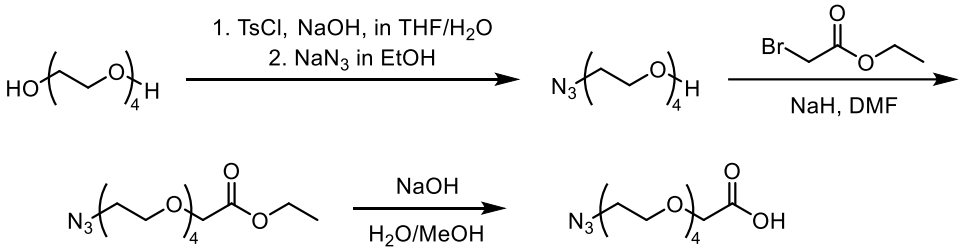

Scheme S3.2: Synthetic scheme for the preparation of linker N_3-PEG_4-COOH.

Preparation of O-(2-azidoethyl)-triethylene glycol (N3-PEG4)

A 250-mL round bottom flask equipped with a magnetic stirring bar was charged with tetraethylene glycol (50.9 g, 262 mmol, 10 eq) in 10 mL tetrahydrofuran. An aqueous solution (10 mL) containing sodium hydroxide (1.68 g, 42 mmol, 1.6 eq) was added to the flask, and p-toluenesulfonyl chloride (5 g, 26.2 mmol, 1 eq) dissolved in 30 mL tetrahydrofuran (THF) was added dropwise over 3h to the mixture maintained at 0˚C. The reaction was diluted with ice-cold water (150 mL) and extracted with 3 x 100 mL dichloromethane. The combined organic layers were washed with 2 x 300 mL of water and once with 100 mL of brine, dried over $MgSO_4$, filtered, and concentrated to yield a clear oil (9.2 g, 26.2 mmol, quantitative yield). Sodium azide (4.3 g, 65.5 mmol, 2.5 eq,) was added to the tosylate intermediate, and the mixture was dissolved in absolute ethanol (200 mL). The reaction was stirred under reflux overnight, cooled to room temperature, and then diluted with water (150 mL). The mixture was concentrated by rotary evaporation to approximately 150 mL, and the product was extracted into ethyl acetate (3 x 150 mL), dried with $MgSO_4$, filtered, and concentrated to yield a faint yellow liquid (5.1 g, 23.3 mmol, 89% yield over two steps). **^{1}H NMR** (300 MHz, $CDCl_3$) δ 3.63 (d, *J* = 4.9 Hz, 12H), 3.59 – 3.54 (m, 2H), 3.40 – 3.31 (m, 2H), 2.69 (s, 1H). **^{13}C NMR** (75 MHz, $CDCl_3$) δ 72.54, 70.74, 70.71, 70.64, 70.40, 70.09, 61.75, 50.71.

Preparation of 14-azido-3,6,9,12-tetraoxatetradecanoic acid (N_3-PEG_4-COOH)

To a dry flask, NaH was added (60% suspension in mineral oil, 0.56 g, 14 mmol, 1.4 eq), and 10 mL dry THF was added to suspend the powder. The reaction was temperature controlled with a water bath and N_3-PEG_4 was added (2,17 g, 10 mmol) in 10 mL dry THF. To the reaction ethyl-bromoacetate (1,67 mL, 15 mmol, 1.5 eq) in 10 mL THF was added dropwise over the course of 30 minutes. The addition funnel was cleaned with a further 5 mL HF, which was also added. The reaction was heated to 50 ˚C and stirred overnight. The reaction was quenched by dropwise addition of ice-cold 90% EtOH/H_2O, and the mixture neutralized to pH 7. The solvent was removed via rotary evaporation, the product dissolved in H_2O, 30 mL and extracted with EtOAc (3 x 30 mL). The solvent was removed yielding a yellowish oil, which was purified via column chromatography using 1:1 Et_2O:ethyl acetate and solvent was removed to yield 903 mg (3 mmol, 30% yield) of an off-white oil. 700 mg (2,3 mmol) of the alkylated PEG was dissolved in 5 mL 96% EtOH, 1,5 mL 5M NaOH was added and the mixture was heated at reflux for 90 minutes. The ethanol was evaporated, the mixture diluted with 8 mL H_2O and washed with 2 x 20 mL DCM. Afterwards, the aq. layer was acidified with acetic acid and extracted with 4 x 20 mL DCM, the organic layers were combined and washed with 10 mL brine, dried with Na_2SO_4 and the solvent removed under vacuum, to yield 640 mg of an off-white oil (quantitative yield). **^{1}H NMR** (300 MHz, $CDCl_3$) δ 4.07 (s, 2H,), 3.70 – 3.47 (m, 14H), 3.33 – 3.23 (t, *J* = 12 Hz, 2H). **^{13}C NMR** (75 MHz, $CDCl_3$) δ 173.73, 70.81, 70.35, 70.29, 70.23, 70.17, 69.75, 68.17, 50.38.

LC-MS of purified peptides

Table S3.6: Overview of the calculated masses of all peptides used in this chapter, and the masses found by LCMS.

Peptide name	Calculated mass (Da)	Measured mass (Da)
K_3GW-1O	$[M + 2H^+]^{2+}$ 1336.77	1335.80
K_3GW-1M	$[M + 2H^+]^{2+}$ 1336.77	1335.31
K_3GW-1P	$[M + 2H^+]^{2+}$ 1336.77	1335.10
K_3GW-2O	$[M + 2H^+]^{2+}$ 1336.77	1336.06
K_3GW-2M	$[M + 2H^+]^{2+}$ 1336.77	1335.57
K_3GW-2P	$[M + 2H^+]^{2+}$ 1336.77	1335.71
K_3GW-3O	$[M + 2H^+]^{2+}$ 1336.77	1335.59
K_3GW-3M	$[M + 2H^+]^{2+}$ 1336.77	1336.01
K_3GW-3P	$[M + 2H^+]^{2+}$ 1336.77	1335.71
K_3GW	$[M + 2H^+]^{2+}$ 1283.27	1281.77
E_3GY	$[M + 2H^+]^{2+}$ 1272.69	1271.70
CP_4-E_3GY	$[M + 2H^+]^{2+}$ 1601.94	1602.13
	$[M + 2H\text{-cholesterol}^+]^{2+}$ 1417.24	1417.01
CP_4-K_3GW	$[M + 2H^+]^{2+}$ 1612.03	1612.06
	$[M + 2H\text{-cholesterol}^+]^{2+}$ 1427.33	1427.22
CP_4-K_3GW-3O	$[M + 2H^+]^{2+}$ 1666.51	1666.21
	$[M + 2H\text{-cholesterol}^+]^{2+}$ 1481.81	1481.51
CP_4-K_3GW-3M	$[M + 2H^+]^{2+}$ 1666.51	1666.35
	$[M + 2H\text{-cholesterol}^+]^{2+}$ 1481.81	1481.65